

Medial Kernels

Matthew Berger^{1,2} and Claudio T. Silva³

¹University of Utah

²Air Force Research Laboratory, Information Directorate

³Polytechnic Institute of New York University

Abstract

We introduce the medial kernel, an association measure which provides for a robust construction of volume-aware distances defined directly on point clouds. The medial kernel is a similarity measure defined as the likelihood of two points belonging to a common interior medial ball. We use the medial kernel to construct a random walk on the point cloud, where movement in the walk is restricted to regions containing similar medial balls. Our distances are defined as the diffusion distances of this random walk, assigning low distance to points belonging to similar medial regions. These distances allow for a robust means of processing incomplete point clouds, capable of distinguishing nearby yet separate undersampled components, while also associating points which are far in Euclidean distance yet mutually share an interior volume. We leverage these distances for several applications: volumetric part segmentation, the construction of function bases, and reconstruction-by-parts – a surface reconstruction method which adheres to the medial kernel.

Categories and Subject Descriptors (according to ACM CCS): I.3.3 [Computer Graphics]: Picture/Image Generation—Line and curve generation

1. Introduction

Advancements in the acquisition of 3D geometry have resulted in the massive proliferation of point clouds. Modern 3D scanners typically acquire point clouds with precise measurement in very little time. However despite these advances, sparse and incomplete data can still be present in the acquisition process. This can be due to the complexity of the shape resulting in occlusion, a wide baseline used in the acquisition such as in stereo systems, or resource constraints resulting in a limited number of scans.

Surface reconstruction in the presence of such data is quite challenging. Methods which employ general smoothness priors [CBC*01, KBH06] are only effective when the priors match the missing data. As a result, much recent work has focused on exploiting the structure of missing data, in order to properly steer surface reconstruction towards a geometric and topologically faithful shape. This can be seen in the recent works of point cloud skeletonization [TZCO09, LLZM10], repetitive structure detection [ZSW*10], visibility carving [SSZCO10], and primitive shape relationships [LWC*11]. At some level, all of these approaches utilize a notion of *distance* with respect to the original point cloud. This may come in the form of k nearest neighbors, ball neighborhoods, and variations which employ normals and primitive shapes. In the presence of miss-

ing data, distance measures which respect the original shape are essential for the success of these methods.

We directly tackle the problem of constructing robust dis-

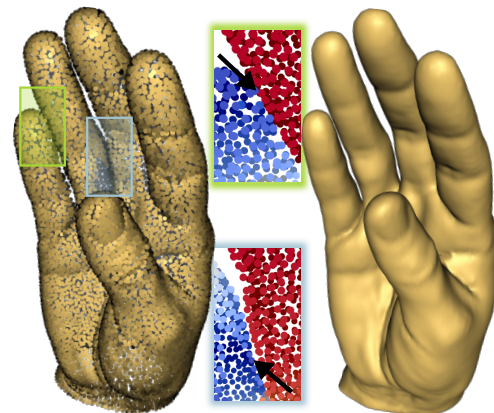


Figure 1: From the input point cloud (left) we show distances derived from the medial kernel, where the arrow highlights the source point. Note the clear separation between the fingers. We use these distances to properly guide surface reconstruction (right).

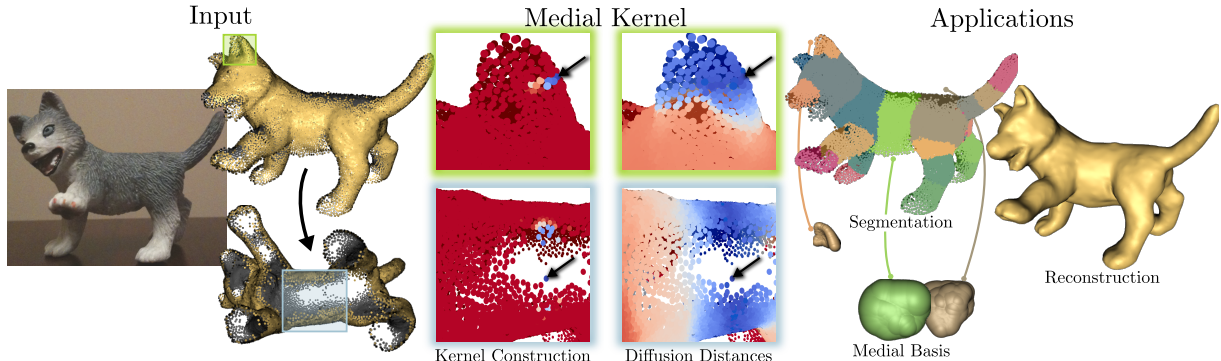


Figure 2: An overview of our approach. From the input point cloud (left), our main contribution is the construction of distances defined directly on the points (middle), where distance represents the likelihood of two points lying on a medial ball. Note the insensitivity to undersampling and missing data. We leverage these distances for several applications, shown on the right.

tances for point clouds. We introduce the *medial kernel*, an association measure which provides for a robust construction of volume-aware distances. To motivate our approach, consider the set of interior medial balls of a surface, that is, balls which are equidistant and tangential to at least two surface points, maximally empty, and inside of the shape. Note that for a smooth surface, the set of medial balls can be represented as a collection of disconnected cliques, where all points which generate a medial ball form a single clique.

For imperfect point clouds containing missing data, finding such cliques can be a challenging task. We instead define a *kernel* on the point cloud, a symmetric nonnegative association measure between every pair of points [CL06]. The kernel measures the likelihood of two points lying on a common interior medial ball – our so-called medial kernel. The medial kernel induces a random walk on the point cloud, such that movement in the walk is restricted to regions containing similar medial balls. In particular, if a subset of points exclusively has a large association according to the medial kernel, then for a sufficiently large time scale the random walk will only permit movement within this subset, effectively forming a clique. Our distance construction follows as the diffusion distances [CL06] of this random walk, where two points contain low distance if they are highly connected in terms of walking along similar medial balls.

Our primary assumption on the input is that there exists sufficient data to indicate a medial structure. As long as this is satisfied, our distance construction is capable of recovering the medial representation through associating points which belong to similar medial regions. See Figure 1 for an illustration of these distances, demonstrating our kernel’s capability to discern the fingers of the hand, despite their close proximity in Euclidean distance and undersampling.

We leverage our medial kernels for several applications – see Figure 2 for an overview. The distances induced by the kernel provide for a simple method of segmenting the point cloud into coherent volumetric parts, even in the pres-

ence of missing data. The medial kernel can be used to construct function bases, where projection onto this basis serves to average function values along medial regions. We use this for surface reconstruction in the presence of missing data. Lastly, we combine these two methods to perform reconstruction-by-parts, a reconstruction method which adheres to the volume indicated by the medial kernel.

2. Related Work

Our approach spans several different areas, each of which we will only discuss the most relevant work due to the lack of space.

Surface Reconstruction: A vast amount of work has been dedicated to surface reconstruction over the past two decades. In the context of handling incomplete point clouds, most existing approaches utilize smooth priors. These range from Poisson surface reconstruction [KHB06], to radial basis functions (RBFs) [CBC^{*}01, OBS04] and partition-of-unity [OBA^{*}03, NOS09]. Recent reconstruction methods have become more specialized, in order to target specific shapes and specific structures in missing data.

Skeleton extraction from incomplete point clouds has seen much work [TZC09, CTO^{*}10, LLZM10]. For the methods of [TZC09, LLZM10], under generalized cylindrical priors reconstruction may be accomplished, but shapes deviating from this prior pose difficulties. The work of [CTO^{*}10] produces skeletons for a more general class of shapes, but resampling missing regions which lack a cylindrical structure still remains a challenge.

Cone carving [SSZCO10] uses visibility cones to properly guide external dipoles for RBF reconstruction. While they produce compelling reconstructions, their approach is sensitive to point splatting, where correct local neighborhoods can be difficult to determine. Our distance construction should serve to aid their point splatting by discarding the influence of neighboring parts.

Similar to our work is [TOZ^{*}11], where they employ volumetric smoothness priors to handle missing data. Our diffusion of medial similarity is also based on an assumption of volumetric smoothness, but we carry out the diffusion algebraically, rather than geometrically.

Medial Representations: Substantial work has been dedicated to extracting medial representations from surfaces, see [SP08] for a thorough overview. One line of work is in representing the surface as the union of medial balls, where various representations may be accomplished by proper scaling/filtering of the medial balls [MGP10]. Such methods rely on extracting a subset of the Voronoi diagram, which is well-defined for ϵ -sampled surfaces, but for point clouds containing missing data the subcomplex of the Voronoi diagram may no longer resemble the medial axis, see [SSZCO10] for an illustration.

In moving away from provably-good approaches, one can obtain more robust methods for medial representations. The shape diameter function [SSCO08] focuses on capturing the overall thickness of the volume, while the part-aware surface metric [LZSCO09] extends this to constructing a volume-dependent metric over the faces of a mesh. Though one may apply such methods to meshes with boundaries, and effectively discard ray samples which do not intersect the surface, for missing data in multiple parts one can easily obtain false volume information. Our construction of the medial kernel is perhaps most aligned with these methods, in that we do not seek *exact* medial balls, but rather approximations and a continuous measure of how far a ball is from medial.

Distances: The construction of distances on surfaces has received much attention as of late. In the case of watertight surface meshes, a slew of useful distances exist, ranging from geodesics, diffusion distances [CL06], killing vector fields [SBCBG11], and biharmonic distances [LRF10], to name a few. These distances are quite useful for performing various shape processing tasks such as segmentation, shape matching, and function interpolation.

For point clouds containing missing data, however, these distances face several problems. As most share the necessity to discretize the Laplace-Beltrami operator on a surface, one may use a method such as [BSW09] for this purpose. But due to isometry-invariance, in the best case the resulting distances will respect the boundary components stemming from the missing data, while in the worst case false connections can result in a fundamentally different, topologically incorrect shape representation.

The work of [CK11] shares similar goals with us, where they employ morphological operators to obtain a watertight representation on which to then construct geodesic distances with respect to the original input. However, dilation/erosion can lead to a topologically incorrect representation, particularly in the presence of nearby surface sheets. Our distances should serve to benefit [CK11], by properly steering these morphological operations.

Our approach is inspired by [LCDF10], where distances are constructed on point clouds encoding *how symmetric* two points are. They observe that points belonging to the same symmetry orbit form cliques in a graph, where by looking at the diffusion distances of a kernel which continuously measures symmetry similarity, one may easily detect these orbits. They illustrate the benefits of working with symmetry-factored distances over symmetry-induced transformations – we leverage the same idea for working with medial-factored distances instead of medial balls.

3. Overview

Before going into the details of our approach we present a brief 2D example illustrating the intuition behind our method, see Figure 3.

Consider the sampled 2D curve on the left-hand side of Figure 3. In observing its set of medial balls, we find that there exists a total of five – two medial balls capping the ends of the shape, and three medial balls towards the center. This information may be encoded as a correspondence matrix C , where C_{ij} is 1 if points i and j belong to the same medial ball, and 0 otherwise. Interpreting C as an adjacency graph, the block structure reveals that we have a disconnected collection of cliques, one clique for every medial ball.

Note that the medial axis can be represented through the spectral properties of C . Under a suitable orthogonal transformation, the eigenvectors of C serve as indicator functions for each medial ball, where for a given eigenvector its nonzero function values group points which lie on the same medial ball. The nonzero eigenvalues of C represent the number of points belonging to a medial ball. If we row-normalize C to obtain \hat{C} , then the multiplicity of eigenvalue with magnitude 1 is the number of medial balls, and consequently the rank of C is the number of medial balls.

Now consider a slight perturbation of this shape, composed of a set of points $P = \{\mathbf{p}_1, \mathbf{p}_2, \dots, \mathbf{p}_k\}$ with accompanying normals $N = \{\mathbf{n}_1, \mathbf{n}_2, \dots, \mathbf{n}_k\}$, where the structure of the cliques is imprecise, see the middle of Figure 3. In this scenario we would like to best recover the cliques and group points which contain a similar medial structure. In other words, we want to approximate the matrix C . Our approach for approximating C is to construct, for a given pair of points in P , a similarity measure representing the likelihood of these two points lying on a medial ball. We call this similarity measure the *medial kernel*, denoted $\phi : P \times P \rightarrow \mathbb{R}$.

Given a pair of points $\mathbf{p}_i, \mathbf{p}_j \in P$ with normals $\mathbf{n}_i, \mathbf{n}_j$, we construct the medial kernel in two steps. First, we generate a *candidate ball*, a representative medial ball for $(\mathbf{p}_i, \mathbf{p}_j)$ being equidistant to \mathbf{p}_i and \mathbf{p}_j and whose normals at the points are similar to \mathbf{n}_i and \mathbf{n}_j . Next, we define a measure of *medial dissimilarity*, or how far away the candidate ball is from being medial. Following the definition of a medial ball, for a candidate ball this is decomposed into two measures: how

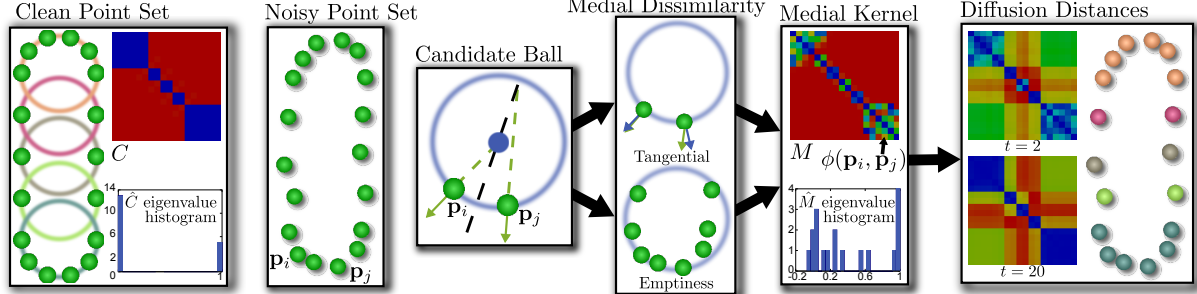


Figure 3: Overview of the medial kernel construction. The clean point set and its set of medial balls illustrates the block structure we would like to recover on the noisy point set. Our medial kernel approximates such correspondences, by measuring the likelihood in which two points contain a medial ball. Note the similarities in spectra between the clean and noisy point sets. We exploit this by applying diffusion distances to the medial kernel to recover the block structure and correspondences.

far from tangential with respect to \mathbf{n}_i and \mathbf{n}_j , and how empty. Emptiness is a function of the number of points residing inside of the ball, and how close they are to the ball center. We then convert this dissimilarity measure into a similarity measure to obtain the medial kernel, see the right side of Figure 3.

From the medial kernel $\phi(\cdot, \cdot)$ we arrive at our approximation to C , the matrix $M : M_{ij} = \phi(\mathbf{p}_i, \mathbf{p}_j)$. Note that nonuniform sampling, positional noise, and normal noise manifests as noise in M . However, similar to [LCDF10], we find that M 's row normalized matrix \hat{M} largely inherits the spectral properties of \hat{C} . This can be seen in the eigenvalues of \hat{M} where its top five eigenvalues reside near 1, and all others quickly converge to 0 – a consequence of the rank deficiency of M . This indicates the existence of five medial balls.

For any shape with a well-defined medial axis, M should exhibit rank deficiency, and we seek to define distances which respect this low rank structure. Note that the medial kernel induces a particular random walk on the point cloud, where for large time scales points walk along similar medial regions. Moreover, a set of points which exclusively contain high associativity in the medial kernel will remain “stuck” in the walk, only moving between each other. Our distance construction follows as the measure of connectedness in this random walk: the diffusion distances [CL06] of M , see the right side of Figure 3. Diffusion distances are a natural tool for recovering such a low-rank structure, in our case grouping together points which mutually contain a similar medial region. Note that unlike the eigenvectors of M , the diffusion distances are invariant to any orthogonal transformation of its eigenspaces [LCDF10]. Observe on the far right that for $t = 20$ we recover the original block structure of C , grouping points which contain similar medial balls.

4. Medial Kernel Construction

Here we describe the details of the medial kernel construction. The medial kernel associates similarity to a pair of

points based on the likelihood of such points containing a medial ball. We construct this by first generating a candidate ball for the points, and then measure how far away this ball is from being a medial ball.

Our construction requires oriented normals N , where we compute normal directions from the input point set P via PCA. If P is obtained from a scanner we use the individual scans to best orient N , otherwise if scan information is unavailable we propagate normal orientation via a minimal spanning tree approach.

4.1. Candidate Ball Generation

For points \mathbf{p}_i and \mathbf{p}_j with normals \mathbf{n}_i and \mathbf{n}_j , we want its candidate ball to best represent an interior medial ball. This implies that the center \mathbf{c}_{ij} lies on the bisecting plane of the points, while the normals of the ball at \mathbf{p}_i and \mathbf{p}_j respectively coincide with \mathbf{n}_i and \mathbf{n}_j .

To this end, we intersect the lines formed from the points and normals against the bisecting plane to obtain intersection points \mathbf{x}_i and \mathbf{x}_j . We discard balls if either intersection is along the positive direction of their normal, indicative of a ball lying in the exterior of the shape, or if both lines fail to intersect the bisecting plane. We would like to have the ball normals at \mathbf{p}_i and \mathbf{p}_j mutually satisfy \mathbf{n}_i and \mathbf{n}_j , but at sharp features this can produce balls of arbitrarily large radius. The inset depicts such a situation, where the right point's normal line fails to intersect the bisecting plane, shown as the dashed black line. Hence we relax this requirement by additionally considering the balls formed by the individual intersection points. This corresponds to the left point's normal intersection with the bisecting plane. So from the points $\{\mathbf{x}_i, \frac{\mathbf{x}_i + \mathbf{x}_j}{2}, \mathbf{x}_j\}$, we take the candidate ball center \mathbf{c}_{ij} as the one with minimal radius, which by construction is equidistant to \mathbf{p}_i and \mathbf{p}_j . Such a hard constraint on point equidistance and soft constraint on normal agreement expresses our precedence for point positions over point normals, since normal estimation is often imperfect.

4.2. Medial Dissimilarity

From the candidate ball, we measure its deviation from a medial ball in two measures: one measures emptiness, while the other measures how tangential.

$$\gamma(\mathbf{p}_i, \mathbf{p}_j) = \sum_{\mathbf{p} \in P} \mu(\mathbf{c}_{ij}, r_{ij}, \mathbf{p}) \quad (1)$$

$$\tau(\mathbf{p}_i, \mathbf{p}_j) = |\mathbf{n}_i - \mathbf{s}_i| + |\mathbf{n}_j - \mathbf{s}_j| \quad (2)$$

Here \mathbf{s}_i and \mathbf{s}_j are the normals of the candidate ball at points \mathbf{p}_i and \mathbf{p}_j , and μ is the *ball distance measure*, measuring how close a point \mathbf{p} lies from the center of the candidate ball \mathbf{c}_{ij} . We would like μ to satisfy the following properties: scale-invariance, slow falloff, and computational efficiency. Scale-invariance implies that the distance measure is relative to the radius of the candidate ball. We want to prescribe a falloff to μ such that points closer to the candidate ball center contribute more, indicative of the ball deeply penetrating the surface. Lastly, μ should be defined such that its summation over all points may be performed efficiently and exactly.

To this end, we define μ as follows:

$$\mu(\mathbf{c}, r, \mathbf{p}) = \begin{cases} 1 - \left(\frac{|\mathbf{p} - \mathbf{c}|}{r} \right)^4 & \text{if } |\mathbf{p} - \mathbf{c}| < r \\ 0 & \text{otherwise} \end{cases} \quad (3)$$

We find that this quartic falloff is suitable for penalizing points which belong in the deep interior of a candidate ball.

Naively evaluating the dissimilarity measure, even using a spatial acceleration structure, can still be linear in the number of points for balls with large radius. However, note that μ can be expanded such that it is linear in \mathbf{c} and powers of \mathbf{c} . To take advantage of this, we construct a kd-tree over P and for each node, precompute its corresponding expansion coefficients over all points which belong to that node. Then in evaluating Equation 2, if a node of the kd-tree is completely contained within a candidate ball, then applying the linear expansion is equivalent to individually summing over all points.

4.3. Medial Kernel

From the measures γ and τ we may now define the medial kernel ϕ , effectively converting medial dissimilarity into a similarity measure:

$$\phi(\mathbf{p}_i, \mathbf{p}_j) = e^{-\left(\frac{\gamma(\mathbf{p}_i, \mathbf{p}_j)}{\sigma_e}\right)^2 - \left(\frac{\tau(\mathbf{p}_i, \mathbf{p}_j)}{\sigma_t}\right)^2} \quad (4)$$

Where σ_e and σ_t define bandwidths for the emptiness and tangential measures, respectively. We have set $\sigma_e = 2$ and $\sigma_t = 0.7$ for all results in the paper, unless otherwise specified. We perform this measure over all point pairs to arrive at the similarity matrix $M : M_{ij} = \phi(\mathbf{p}_i, \mathbf{p}_j)$, where each entry encodes how likely the point pair contains a medial ball.

In practice we find most entries of M to have small magnitude – a function of the complexity of the medial axis. Hence

we set M_{ij} to 0 if $M_{ij} < 10^{-7}$, resulting in M typically being quite sparse. We use this sparsity to employ an early termination in the traversal of the kd-tree for computing the emptiness measure γ , allowing us to quickly discard point pairs which are highly dissimilar.

The matrix M can be quite noisy. For instance, since we have a hard constraint on equidistance in candidate ball generation, two adjacent points lying on a plane will result in a ball with unbounded radius, and consequently low similarity. However, if two such points mutually share other points which have a high similarity, then there is a strong likelihood that these points belong to the same medial ball.

As discussed in Section 3, the diffusion maps of M capture this similarity, in the form of measuring the connectedness of random walks defined via the medial kernel. To this end, consider the matrix \hat{M} taken as the row-normalization of M , as suggested by [CL06, LCDF10]. It has an eigen-decomposition of the form $\hat{M} = V\Sigma U^T$, where its eigenvalues and left/right eigenvectors are real-valued. Letting $V = [\Psi_1 \Psi_2 \dots \Psi_k]$, the resulting diffusion map at point \mathbf{p}_i under a time scale t is:

$$\Phi_t(\mathbf{p}_i) = \{\lambda_1^t \Psi_1(\mathbf{p}_i), \lambda_2^t \Psi_2(\mathbf{p}_i), \lambda_3^t \Psi_3(\mathbf{p}_i), \dots\} \quad (5)$$

The diffusion distances directly follow from Φ :

$$d_t^2(\mathbf{p}_i, \mathbf{p}_j) = |\Phi_t(\mathbf{p}_i) - \Phi_t(\mathbf{p}_j)|^2 \quad (6)$$

Unless otherwise specified we used a time scale of $t = 160$ for all results, which we found to be a conservative time scale as useful distances are typically achieved at smaller times. Due to the large time scale used, we found it necessary to only retain the top 300 eigenvectors, and since M is sparse this can be computed efficiently via ARPACK.

See Figure 4 for several examples of diffusion distances of the medial kernel. Note how the distances relate points which have high likelihood of belonging to an underlying medial ball, for both well-sampled shapes and single range scans alike. Figure 5 illustrates our ability to handle the case of two nearby planar surface sheets. Note that although adjacent planar points are initially dissimilar, under a suitable

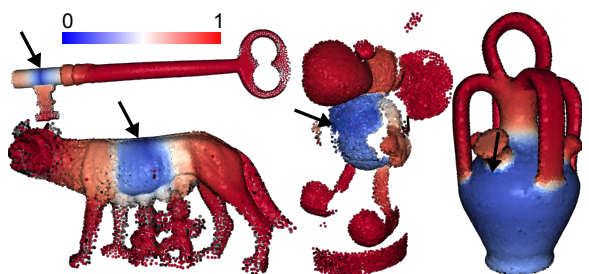


Figure 4: Diffusion distances derived from the medial kernel from various source points for a variety of point clouds, ranging from fully-sampled meshes to single range scans.

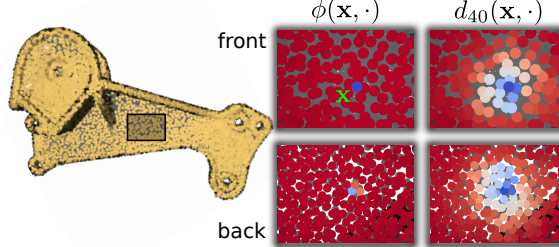


Figure 5: Distances constructed on thin planar sheets. Although adjacent points to \mathbf{x} are initially dissimilar, diffusion distances capture the association from the other side of the surface for suitably large times.

time-scale we are able to capture the similarity, indicative of a medial ball lying between the surface.

Figure 6 shows the kernel’s robustness to missing data and noise. Note that noise is both positional and normal, since we compute normals from the points via PCA. This is a particularly challenging model as the foot resides directly next to the leg of the dancer, with missing data between the two parts. As noise increases, our method is still able to associate similarity to points occupying similar volume, as points on the back of the leg contain small distance to the source point.

5. Applications

We illustrate several applications of the medial kernel: segmenting a point cloud into volumetric parts, “medializing” functions by deriving a function basis from the medial kernel, and reconstruction-by-parts.

5.1. Volume-Aware Segmentation

For large time scales, the diffusion distances of the medial kernel serve to associate similarity to points which contain smoothly varying volumetric emptiness. Based on this observation, we can easily perform point cloud segmentation

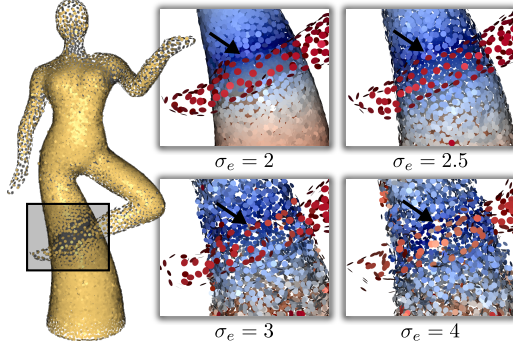


Figure 6: The performance of our medial kernel under missing data and increasing noise. Note that the source point contains low distance to points occupying similar volume.

using the medial kernel, where points are segmented into clusters occupying similar volumes.

We achieve this segmentation by performing k -means on the diffusion maps, defined by Equation 5. We normalize the coordinates prior to clustering, similar to existing methods [ZMP04, SBCBG11]. The resulting segmentation is not intended to be a semantic part decomposition, but rather a decomposition into simple and coherent volumetric parts. In particular, the main contribution is segmentation in the presence of missing data, see Figure 7 for an illustration. The segmentation properly clusters the palm into separate parts, separating it from the two fingers despite the fact that there exists no data underneath the fingers.

5.2. Medial Basis

In addition to constructing random walks, the medial kernel can also be used to define a basis from which to project functions onto, in a similar manner to [LCDF10]. In particular, powers of the matrix \hat{M} correspond to a family of such bases, where for a large t , \hat{M}^t serves to effectively reduce the numerical rank of \hat{M} . Recall that the numerical rank of \hat{M}^t reflects the complexity of the shape’s medial axis. The linear subspace of functions spanned by \hat{M}^t correspond to functions which are constant along medial balls. Hence, for an arbitrary function f its projection onto \hat{M}^t serves to diffuse function values along medial balls, in the process “medializing” f .

More specifically, from the diagonalization of $\hat{M} = V\Sigma U^T$, suppose we have the set of right eigenvectors $U = [\Theta_1 \Theta_2 \dots \Theta_k]$. Powers of \hat{M} may be expressed as:

$$\hat{M}^t = \sum_i \Psi_i \lambda_i^t \Theta_i^T \quad (7)$$

Then the projection of f onto \hat{M}^t is:

$$\hat{M}^t f = \sum_i \Psi_i \lambda_i^t \langle \Theta_i^T, f \rangle \quad (8)$$

Diffusion of Union of Balls (DUB): In considering useful functions to medialize, we observe that one should choose

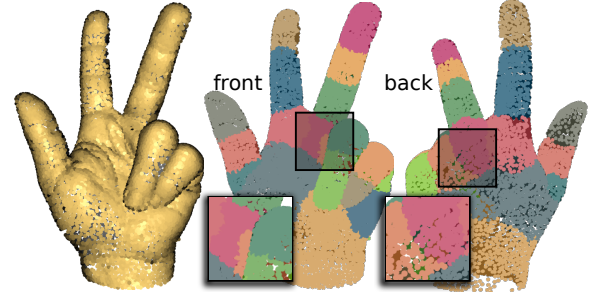


Figure 7: Segmentation results on a hand point cloud (left). Note that the knuckle of the ring finger is properly associated with the palm, despite the lack of data on the palm.

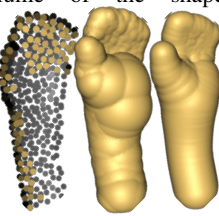
functions which are naturally invariant to the medial basis, yet are initially noisy. The union of balls [MGP10], i.e. the set of interior medial balls, is thus a natural candidate. This provides us with a simple yet robust method for reconstruction, which we term the Diffusion of Union of Balls (DUB).

In our approximate scenario, we derive the initial set of balls from our construction of the kernel. For a given point \mathbf{p}_i , we define its initial ball $[\mathbf{c}_i, r_i]$ as:

$$\mathbf{c}_i = \frac{\sum_j \mathbf{c}_{ij} \phi(\mathbf{p}_i, \mathbf{p}_j)}{\sum_j \phi(\mathbf{p}_i, \mathbf{p}_j)} \quad r_i = \frac{\sum_j r_{ij} \phi(\mathbf{p}_i, \mathbf{p}_j)}{\sum_j \phi(\mathbf{p}_i, \mathbf{p}_j)} \quad (9)$$

Assuming that \mathbf{c} and \mathbf{r} refer to the set of ball centers and radii defined over the point set, respectively, then its diffusion over the medial basis is: $\mathbf{c}' = \hat{M}^t \mathbf{c}$ and $\mathbf{r}' = \hat{M}^t \mathbf{r}$.

As long as there exists sufficient evidence of a volume, we find that DUB is quite effective at preserving the overall volume of the shape. Refer to the inset for an illustration, where we apply DUB for times $t = 0$ and $t = 5$. Note how despite the missing data, by projecting onto \hat{M} we are able to sufficiently smooth out the noise. We note that this method is similar to VASE [TOZ*11], in that we both rely on smoothness in the volume to diffuse a medial representation. However, we define a diffusion operator on the point cloud, rather than an intermediate mesh representation.



5.3. Reconstruction by Parts

Although DUB is effective when the initial set of balls is noisy, if the basis is also noisy then the diffusion can produce undesirable results due to the contamination of dissimilar balls. The mid-left image of Figure 8 depicts the situation, where false positives exist between the hand and the body of the dancer, causing a tunnel to appear in the reconstruction. However, this is precisely what our segmentation method resolves: the clustering of the point cloud into coherent volumetric parts. Hence it is natural to combine the two methods, resulting in a surface reconstruction method which performs reconstruction-by-parts. See Figure 8 for an illustration.

We first segment the point cloud into volumetric components via k -means. The number of clusters should be large enough so that nearby parts are separated, yet not so big that there exists an insufficient number of points to represent a volume. For most shapes this range is typically quite large, however, and for all results in the paper we found 20–30 segments to be sufficient. We next pad each segment out with points belonging to other segments which are close in terms of our medial-factored distances. We achieve this by performing a k -nearest neighbors query with respect to the diffusion map across all of the points in a segment, adding points which belong to different segments. We choose $k = 25$

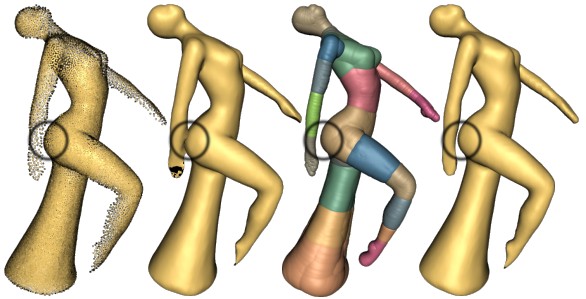


Figure 8: From the point cloud on the left, we first show the reconstruction through Diffusion of Union of Balls (DUB) on the entire point cloud, followed by projection (mid-left). Note the tunnel introduced due to false positives in our kernel. By segmenting the point cloud (mid-right) and then performing reconstruction-by-parts, we produce a topologically accurate reconstruction (right).

in our implementation, which we have found to provide for sufficient overlap between segments.

We then apply DUB to each segment, to obtain a collection of union of balls. Our volumetric segmentation ensures that each DUB-reconstructed segment encompasses a proper volume of the shape, where we found time scale $t = 4$ to provide for a smooth yet geometrically faithful representation for each segment. We then take the union of the union of balls as our reconstructed mesh. Namely, we treat all of the union of balls as an implicit surface and isosurface to obtain the reconstructed mesh. Since we are padding each segment with points in nearby segments (with respect to medial-factored distances), there exists sufficient overlap between individual reconstructions to form a single component.

The resulting mesh is slightly shrunken due to the diffusion process. We obtain the final reconstruction by interleaving MLS projection (via Algebraic Point Set Surfaces [GG07]) and least squares meshes [SCOIT05], applied to the vertices of the mesh, in a similar manner to [SLS*06]. We depart from [SLS*06] by restricting the projection step to the individual clusters, in order to prevent projection issues associated with undersampling of the point cloud.

6. Results

We compare our approach to kernel methods regarding distances and segmentation, as well as to reconstruction methods. Most point clouds used in the paper have been acquired either through NextEngine or Kreon scanners, and consequently downsampled through farthest point sampling. No data smoothing is employed in the downsampling, we use the original points and normals.

Kernel Methods: We first compare the diffusion distances of our medial kernel to a more standard kernel, namely the feature-preserving kernel of [OAG10] which approximates the heat kernel for point clouds. Note that the

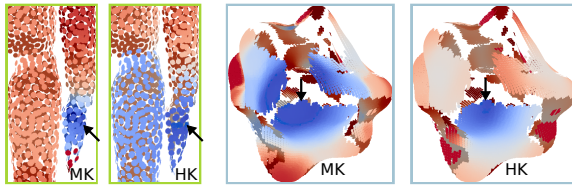


Figure 9: A comparison of distances between our kernel (MK) and the kernel of [OAG10] (HK), both under large-time diffusion distances. Note that the kernel of [OAG10] can leak into other parts of the shape (left) while not adequately covering distant sheets (right). Our method properly handles both cases.

heat kernel is well known to be robust to missing data and topological shortcuts, as demonstrated for segmentation of surface meshes in [DGGV08]. For point clouds the approach of [OAG10] constructs the kernel as:

$$k(\mathbf{p}_i, \mathbf{p}_j) = e^{-\left(\frac{|\mathbf{p}_i - \mathbf{p}_j|}{\sigma_p}\right)^2 - \left(\frac{|\mathbf{n}_i - \mathbf{n}_j|}{\sigma_n}\right)^2} \quad (10)$$

Originally used for its short-time behavior, we consider its long-time behavior in diffusion distances. We set σ_p to 0.02 of the bounding box diagonal, and σ_n to 0.5, a small bandwidth which heavily penalizes normal differences [OAG10].

See Figure 9 for a comparison between distances. The Mannequin model highlights the issues with thin sheets, where although both methods contain false positives, our method successfully filters them out since the connectedness induced by medial balls is stronger. The Bumpy Sphere model highlights the opposite issue: points which are outside of the bandwidths of σ_p and σ_n are never connected, hence the kernel of [OAG10] retains the boundary components. Our method identifies the presence of a medial ball connecting the three disparate sheets. Figure 10 shows how this type of identification results in a volumetric segmentation, whereas k -means applied to [OAG10] keeps these parts separate.

Comparison to Killing Vector Fields: Our method bears resemblance to the recent work on mesh segmentation via killing vector fields (KVF) [SBCBG11]. A KVF defines an isometric self-mapping, where [SBCBG11] show how the eigenfunctions of a suitable KVF energy can be used to localize self-isometries for segmentation. For large time scales, our method begins to resemble local self-isometries, as the medial ball itself can be looked upon as a local transformation. Indeed, our segmentation approach of clustering (weighted) eigenvectors of a point cloud operator mirrors [SBCBG11], and as the inset shows we obtain nearly identical segmentations for the given model. It would be interesting future work to extend [SBCBG11] to the case of incomplete point clouds via our method.

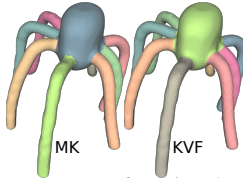


Figure 10: K -means segmentation applied to our method (MK) and the kernel of [OAG10] (HK). Note how our segmentation captures the body of the wolf, despite the large missing data.

Surface Reconstruction: We have ran our reconstruction algorithm on a set of challenging acquired data, containing missing data and thin surface sheets. In these scenarios, an explicit segmentation of these regions substantially simplifies reconstruction. We show that our distances provide for a robust means of achieving this segmentation and generating a faithful reconstruction.

See Figure 11 for a comparison of our method with that of Fourier surface reconstruction [Kaz05], adaptive RBFs [OBS04], and smoothed MPU [NOS09]. One potential issue with these methods is that they employ function fitting [OBS04, NOS09] or variational reconstruction [Kaz05] independent of the structure of the point cloud. Hence for thin sheets with missing data there are no constraints on the surface produced. By segmenting the point cloud via the medial kernel, we avoid issues related to missing data and undersampling.

Our method is also robust to the number of segments used for reconstruction. See Figure 12 for an illustration of the hand point cloud (from Figure 1) reconstructed under different numbers of clusters. As shown, the reconstruction is largely unaffected by the different number of clusters.

Discussion and Limitations: Our medial kernel relies on sufficient evidence of a medial structure for success, so in this absence our method will result in either isolated points or false positives. The former case does not pose much of a problem in the context of distances and segmentation, but for reconstruction it may be difficult to construct an initial set of union-of-balls. In the latter case, false positives typically occur when neighboring parts have insufficient data to penalize candidate balls between the parts.

Our kernel construction requires oriented normals, where although it is quite robust to normal directions (see Figure 6), it is somewhat sensitive to inverted orientation. Our approach can tolerate a small amount of inverted orientation, but for large and continuous regions of inverted normals we begin to interpret exterior medial balls as being interior.

Perhaps the biggest drawback to our approach is its computational complexity. To construct our measure of emptiness we must consider, for every pair of points, the entire point set. Hence in the worst case the complexity is cubic in

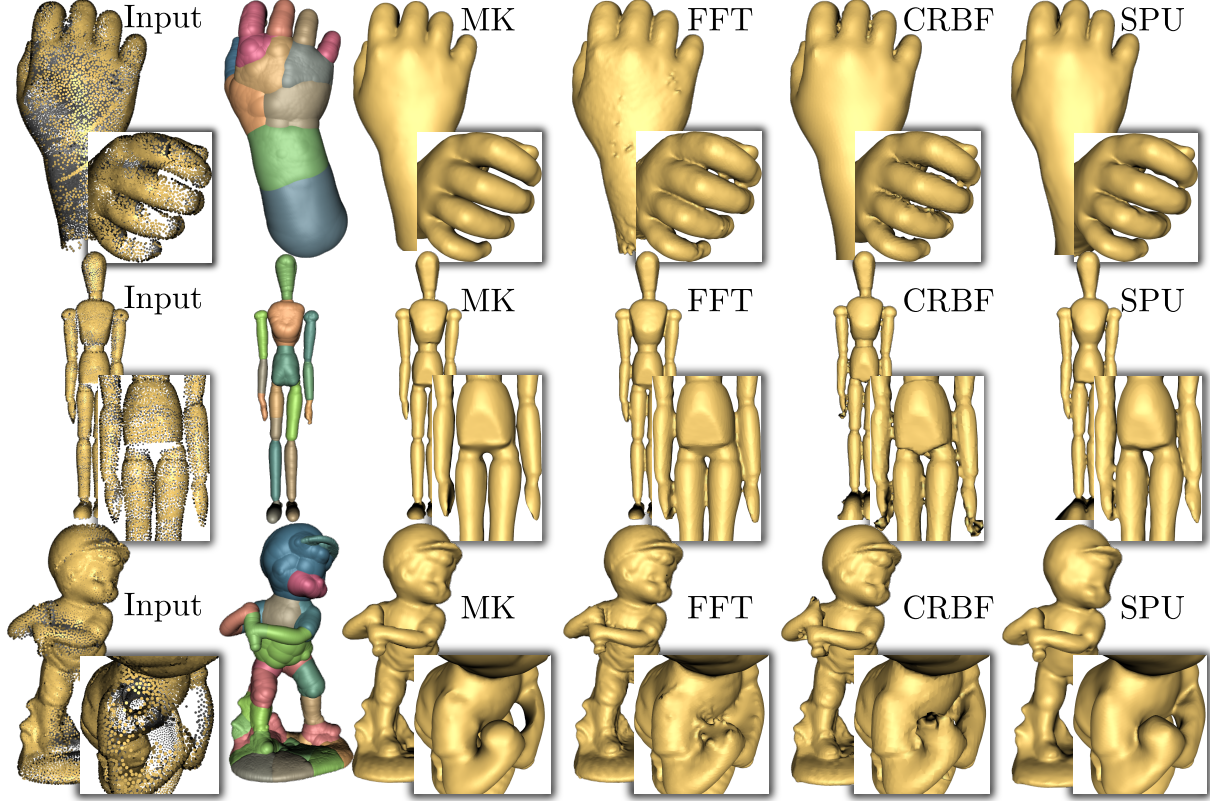


Figure 11: Comparison of surface reconstruction. We first show our reconstruction by way of segmentation, and then a comparison of our method to FFT [Kaz05], CRBF [OBS04], and SPU [NOS09]. Since our method explicitly segments parts of the point cloud, we avoid issues related to missing data and thin surface sheets, where previous methods contain difficulties.

the number of points. However in practice, our acceleration scheme typically provides an order of magnitude improvement. Figure 13 shows computational timings as a function of point cloud size, and as shown the kernel construction is generally quadratic. We find that our acceleration scheme is slowest when dealing with spherical parts of a shape, since for these points the kernel measure is high and so we must sum over all other points on the part to obtain an accurate

measure. This is the cause of the Batter model being so time consuming, due to the head part. However, a voting scheme analogous to [LCDF10] should considerably speed this up.

7. Conclusions

We have presented medial kernels, a method for constructing robust distances on point clouds containing incomplete data.

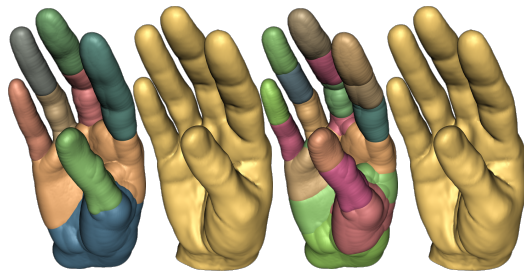


Figure 12: From the point cloud in Figure 1, we show segmentations of different cluster sizes, and the reconstructions. Note the insensitivity to the number of clusters.

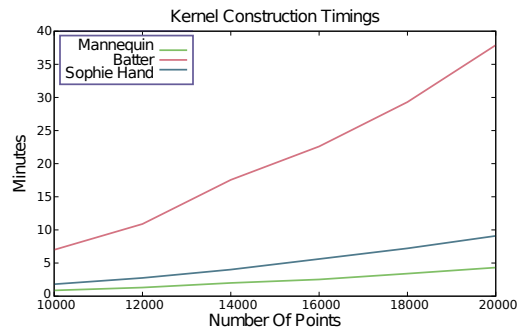


Figure 13: Timings for kernel construction on the shapes used in Figure 11, as a function of point cloud size.

Our key idea is the construction of a medial representation through diffusion distances directly on the point cloud. We have illustrated its robustness, as well its application towards segmentation, function bases, and reconstruction.

For future work we hope to extend the kernel construction to large-scale, raw point clouds by utilizing a voting scheme to efficiently compute our emptiness measure. As the construction of our kernel is quite simple, we think it may be possible to derive explicit bounds on how much missing data our distances can tolerate. Our kernel should also prove useful in other areas outside of reconstruction, where we intend to apply the kernel to registration and deformation.

Acknowledgements

We thank Justin Solomon for the KVF comparison and Shy Shalom for the Mannequin point cloud. This work was partially funded by the National Science Foundation and the Department of Energy Office of Science.

References

- [BSW09] BELKIN M., SUN J., WANG Y.: Constructing laplace operator from point clouds in rd. In *Proceedings of the twentieth Annual ACM-SIAM Symposium on Discrete Algorithms* (Philadelphia, PA, USA, 2009), SODA '09, Society for Industrial and Applied Mathematics, pp. 1031–1040.
- [CBC*01] CARR J., BEATSON R., CHERRIE J., MITCHELL T., FRIGHT W., MCCALLUM B., EVANS T.: Reconstruction and representation of 3d objects with radial basis functions. In *Proceedings of the 28th annual conference on Computer graphics and interactive techniques* (2001), ACM, pp. 67–76.
- [CK11] CAMPEN M., KOBBELT L.: Walking on broken mesh: Defect-tolerant geodesic distances and parameterizations. In *Computer Graphics Forum* (2011), vol. 30, pp. 623–632.
- [CL06] COIFMAN R., LAFON S.: Diffusion maps. *Applied and Computational Harmonic Analysis* 21, 1 (2006), 5–30.
- [CTO*10] CAO J., TAGLIASACCHI A., OLSON M., ZHANG H., SU Z.: Point cloud skeletons via laplacian based contraction. In *IEEE Shape Modeling International* (2010), pp. 187–197.
- [DGGV08] DE GOES F., GOLDENSTEIN S., VELHO L.: A hierarchical segmentation of articulated bodies. In *Computer Graphics Forum* (2008), vol. 27, pp. 1349–1356.
- [GG07] GUENNEBAUD G., GROSS M.: Algebraic point set surfaces. In *ACM SIGGRAPH 2007 papers* (2007), ACM, pp. 23:1–23:10.
- [Kaz05] KAZHDAN M.: Reconstruction of solid models from oriented point sets. In *Proceedings of the Symposium on Geometry Processing* (2005), pp. 73–82.
- [KBH06] KAZHDAN M., BOLITHO M., HOPPE H.: Poisson surface reconstruction. In *Proceedings of the Symposium on Geometry Processing* (2006), pp. 61–70.
- [LCDF10] LIPMAN Y., CHEN X., DAUBECHIES I., FUNKHOUSER T.: Symmetry factored embedding and distance. In *ACM SIGGRAPH 2010 papers* (New York, NY, USA, 2010), SIGGRAPH '10, ACM, pp. 103:1–103:12.
- [LLZM10] LI G., LIU L., ZHENG H., MITRA N. J.: Analysis, reconstruction and manipulation using arterial snakes. *ACM Trans. Graph.* 29 (December 2010), 152:1–152:10.
- [LRF10] LIPMAN Y., RUSTAMOV R. M., FUNKHOUSER T. A.: Biharmonic distance. *ACM Trans. Graph.* 29 (July 2010), 27:1–27:11.
- [LWC*11] LI Y., WU X., CHRYSATHOU Y., SHARF A., COHEN-OR D., MITRA N. J.: Globfit: consistently fitting primitives by discovering global relations. *ACM Trans. Graph.* 30 (August 2011), 52:1–52:12.
- [LZSCO09] LIU R., ZHANG H., SHAMIR A., COHEN-OR D.: A part-aware surface metric for shape analysis. In *Computer Graphics Forum* (2009), vol. 28, pp. 397–406.
- [MGP10] MIKLOS B., GIESEN J., PAULY M.: Discrete scale axis representations for 3d geometry. *ACM Trans. Graph.* 29 (July 2010), 101:1–101:10.
- [NOS09] NAGAI Y., OHTAKE Y., SUZUKI H.: Smoothing of partition of unity implicit surfaces for noise robust surface reconstruction. In *Computer Graphics Forum* (2009), vol. 28, pp. 1339–1348.
- [OAG10] ÖZTIRELI A. C., ALEXA M., GROSS M.: Spectral sampling of manifolds. In *ACM SIGGRAPH Asia 2010 papers* (New York, NY, USA, 2010), ACM, pp. 168:1–168:8.
- [OBA*03] OHTAKE Y., BELYAEV A., ALEXA M., TURK G., SEIDEL H.: Multi-level partition of unity implicits. In *ACM Trans. Graph.* (2003), vol. 22, ACM, pp. 463–470.
- [OBS04] OHTAKE Y., BELYAEV A., SEIDEL H.: 3d scattered data approximation with adaptive compactly supported radial basis functions. In *Proceedings of Shape Modeling Applications*. (2004), pp. 31–39.
- [SBCBG11] SOLOMON J., BEN-CHEN M., BUTSCHER A., GUIBAS L.: Discovery of intrinsic primitives on triangle meshes. In *Computer Graphics Forum* (2011), vol. 30, pp. 365–374.
- [SCOTI05] SORKINE O., COHEN-OR D., IRONY D., TOLEDO S.: Geometry-aware bases for shape approximation. *IEEE Transactions on Visualization and Computer Graphics* (2005), 171–180.
- [SLS*06] SHARF A., LEWINER T., SHAMIR A., KOBBELT L., COHEN-OR D.: Competing fronts for coarse-to-fine surface reconstruction. In *Computer Graphics Forum* (2006), vol. 25, pp. 389–398.
- [SP08] SIDDIQI K., PIZER S.: *Medial representations: mathematics, algorithms and applications*, vol. 37. Springer Verlag, 2008.
- [SSCO08] SHAPIRA L., SHAMIR A., COHEN-OR D.: Consistent mesh partitioning and skeletonisation using the shape diameter function. *The Visual Computer* 24, 4 (2008), 249–259.
- [SSZCO10] SHALOM S., SHAMIR A., ZHANG H., COHEN-OR D.: Cone carving for surface reconstruction. In *ACM SIGGRAPH Asia 2010 papers* (New York, NY, USA, 2010), ACM, pp. 150:1–150:10.
- [TOZ*11] TAGLIASACCHI A., OLSON M., ZHANG H., HAMARNEH G., COHEN-OR D.: Vase: Volume-aware surface evolution for surface reconstruction from incomplete point clouds. In *Computer Graphics Forum* (2011), vol. 30, pp. 1563–1571.
- [TZCO09] TAGLIASACCHI A., ZHANG H., COHEN-OR D.: Curve skeleton extraction from incomplete point cloud. *ACM Trans. Graph.* 28 (July 2009), 71:1–71:9.
- [ZMP04] ZELNIK-MANOR L., PERONA P.: Self-tuning spectral clustering. *Advances in neural information processing systems* 17, 1601–1608 (2004), 16.
- [ZSW*10] ZHENG Q., SHARF A., WAN G., LI Y., MITRA N. J., COHEN-OR D., CHEN B.: Non-local scan consolidation for 3d urban scenes. *ACM Trans. Graph.* 29 (July 2010), 94:1–94:9.